A numerical study on the effect of hydrogen/reformate gas addition on flame temperature and NO formation in strained methane/air diffusion flames

Guo, Hongsheng; Neill, W. Stuart

Publisher's version / Version de l'éditeur:
https://doi.org/10.1016/j.combustflame.2008.07.009
Combustion and Flame, 156, 2, pp. 477-483, 2009

Combustion and Flame 156 (2009) 477–483

Contents lists available at ScienceDirect

Combustion and Flame

www.elsevier.com/locate/combustflame

A numerical study on the effect of hydrogen/reformate gas addition on flame temperature and NO formation in strained methane/air diffusion flames

Hongsheng Guo *, W. Stuart Neill

Institute for Chemical Process and Environmental Technology, National Research Council Canada, 1200 Montreal Road, Ottawa, Ontario, K1A 0R6, Canada

ARTICLE INFO

Article history:
Received 5 May 2008
Received in revised form 28 July 2008
Accepted 30 July 2008
Available online 27 August 2008

Keywords:
Fuel enrichment
Hydrogen
Reformate gas
Super-adiabatic temperature
NO_x

ABSTRACT

This paper investigates the effects of hydrogen/reformate gas addition on flame temperature and NO formation in strained methane/air diffusion flames by numerical simulation. The results reveal that flame temperature changes due to the combined effects of adiabatic temperature, fuel Lewis number and radiation heat loss, when hydrogen/reformate gas is added to the fuel of a methane/air diffusion flame. The effect of Lewis number causes the flame temperature to increase much faster than the corresponding adiabatic equilibrium temperature when hydrogen is added, and results in a qualitatively different variation from the adiabatic equilibrium temperature as reformate gas is added. At some conditions, the addition of hydrogen results in a super-adiabatic flame temperature. The addition of hydrogen/reformate gas causes NO formation to change because of the variations in flame temperature, structure and NO formation mechanism, and the effect becomes more significant with increasing strain rate. The addition of a small amount of hydrogen or reformate gas has little effect on NO formation at low strain rates, and results in an increase in NO formation at moderate or high strain rates. However, the addition of a large amount of hydrogen increases NO formation at all strain rates, except near pure hydrogen condition. Conversely, the addition of a large amount of reformate gas results in a reduction in NO formation.

1. Introduction

Hydrogen enrichment is a promising concept for reducing fuel consumption and pollutant emissions. It has been shown that hydrogen enrichment can improve flame stability and thus reduce NO_x formation in premixed flames [1–5], as well as increase burning velocity [6–8]. For diffusion combustion, hydrogen enrichment can suppress the formation of soot particles [9,10] and shorten ignition delay [11,12].

Relatively, not enough attention has been paid to the effect of hydrogen enrichment on NO_x formation in diffusion flames. When hydrogen is added to a hydrocarbon diffusion flame, it is expected that the NO formation rate by the prompt route is reduced. On the other hand, the addition of hydrogen may modify flame temperature, which in turn may change NO formation rate by the thermal route. The net effect of hydrogen enrichment on NO formation in a hydrocarbon diffusion flame depends on the relative variations of the thermal and prompt routes. Naha and Aggarwal [13] investigated the effect of hydrogen addition on NO_x formation in strained nonpremixed methane and *n*-heptane flames at a fixed strain rate (100 s^{-1}). They found that the addition of hydrogen had a minor effect on NO formation in methane flames and reduced the formation of NO in *n*-heptane flames. The variation in strain rate modifies the residence time of reactants in the reaction zone of a flame, and thus affects NO_x formation mechanism [14]. The effect of hydrogen enrichment on NO_x formation depends on strain rates. Therefore, it is of great interest to further investigate the effect of hydrogen addition on NO_x formation in diffusion flames at various strain rates.

Besides, hydrogen is an energy carrier, and has to be obtained from other hydrocarbon fuels or water. One way to generate hydrogen is fuel reforming. The product of fuel reforming, known as reformate gas (RG), contains not only hydrogen, but also carbon monoxide and some other components. Instead of using hydrogen, it is more practical and economical to directly use RG for fuel enrichment. In addition, the study of RG enrichment combustion is directly related to the application of syngas that is an important alternative fuel. Therefore, it is also of practical importance to investigate the effect of RG addition.

This paper presents a detailed numerical study on the effect of hydrogen and RG addition to fuel on NO formation in laminar methane/air diffusion flames at different strain rates. Since NO_x formation is closely related to flame temperature, the effect of hydrogen and RG addition on temperature is also examined. Methane was selected as the base fuel, because its reaction scheme is rela-

* Corresponding author. Fax: +1 (613) 957 7869.
E-mail address: hongsheng.guo@nrc-cnrc.gc.ca (H. Guo).

0010-2180/$ – see front matter
doi:10.1016/j.combustflame.2008.07.009

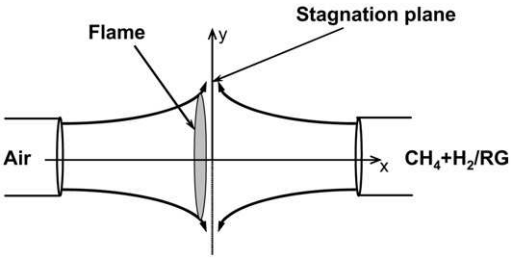

Fig. 1. Flame configuration.

tively well known. The study is limited to NO formation, the main component of NO_x.

2. Numerical model

The flame configuration studied is a traditional axisymmetric laminar counterflow diffusion flame, as shown in Fig. 1. By assuming the stagnation point flow approximation [15], the governing equations are written as

$$\frac{d\rho}{dt}+\frac{dV}{dx}=-2\rho G, \tag{1}$$

$$L(G)=\frac{d}{dx}\left(\mu\frac{dG}{dx}\right)-\rho G^2+\rho\left(\frac{da}{dt}+a^2\right), \tag{2}$$

$$C_pL(T)=\frac{d}{dx}\left(\lambda\frac{dT}{dx}\right)-\sum_{k=1}^{KK}\rho Y_kV_kC_{pk}\frac{dT}{dx}-\sum_{k=1}^{KK}h_k\omega_kM_k+q_r, \tag{3}$$

$$L(Y_k)=-\frac{d}{dx}(\rho Y_kV_k)+\omega_kM_k, \tag{4}$$

where $L(\phi)=d\phi/dt+V(d\phi/dx)$; t is the time; x is the axial coordinate; V is the axial mass flow rate and a is the strain rate. Quantity G is a combined function of the strain rate and the stream function; ρ is the density of the mixture; T the temperature; Y_k the mass fraction of the kth species; μ the viscosity of the mixture; C_{pk} the constant pressure heat capacity of the kth species; M_k the molecular weight of the kth species; h_k, V_k and ω_k are, respectively, the species enthalpy, the diffusion velocity and the molar production rate of the kth species; and KK the total species number; and q_r is the term due to radiation heat loss.

The potential boundary condition was used. They are given as:

$$x=x_{\text{air}};\qquad T=T_{\text{air}},\quad Y_k=Y_{k,\text{air}},\quad G=a\sqrt{\frac{\rho_{\text{fuel}}}{\rho_{\text{air}}}},\quad V=V_{\text{air}},$$

$$x=x_{\text{fuel}};\qquad T=T_{\text{fuel}},\quad Y_k=Y_{k,\text{fuel}},\quad G=a,\quad da/dt=0.0$$

where x_{air} and x_{fuel} represent the axial positions of air and fuel nozzles, respectively.

The calculations were carried out with a code revised from that of Kee et al. [16] for counterflow flame configuration. In the code, upwind and central difference schemes are used for the convective and diffusion terms, respectively, in all the governing equations. Adaptive mesh refinement is done to obtain grid independent results. Radiation heat loss is accounted for by an optically thin model [17], considering radiation from species CH_4, CO, CO_2 and H_2O. The reaction mechanism used is GRI-Mech 3.0 [18], which has been shown to offer reasonable prediction of NO formation for various flames [19,20]. The thermal and transport properties are obtained by using the database of GRI-Mech 3.0 and the algorithms given in [21,22]. Both ordinary and thermal diffusion are taken into account. The multicomponent formulation [21] is employed for the calculation of diffusion velocities. The distance between the two nozzles was maintained as 4.0 cm in all the calculations, while the mass flow rate of air (V_{air}) was varied so that the stagnation plane is located near the middle of the two nozzles.

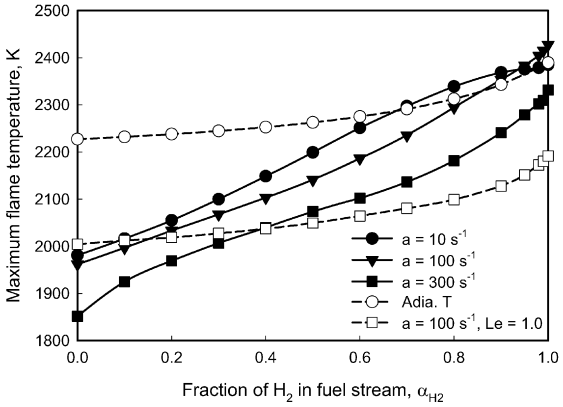

Fig. 2. Effect of hydrogen addition on flame temperature. Solid lines with filled symbol: temperatures at different strain rates; Dashed line with open circle: equilibrium adiabatic temperature of the stoichiometric mixture (R1) at corresponding α_{H_2}; Dashed line with open square: temperatures of flames at strain rate of 100 s^{-1} and with Le of all species being artificially set to unity.

The pressure and the fresh mixture (both air and fuel stream) temperature are 1 atm and 298 K, respectively. While hydrogen or RG is gradually added to the fuel stream, air is maintained as the oxidant. The RG is assumed to be the product of partial oxidation of methane by air via the reaction $2CH_4+O_2+\frac{79}{21}N_2=2CO+4H_2+\frac{79}{21}N_2$. Therefore, the RG contains not only H_2 and CO but also N_2. The volume composition of the RG is $(42CO+84H_2+79N_2)/205$. The fraction of enrichment additive, α_{H_2} or α_{RG}, is defined as the volume fraction of H_2 or RG in the fuel stream, i.e. the ratio of H_2 or RG volume flow rate to the sum of CH_4 and H_2 or RG volume flow rates.

The complete combustion of the fuel mixture in air at stoichiometric condition goes via reactions

$$(1-\alpha_{H_2})CH_4+\alpha_{H_2}H_2+\frac{4-3\alpha_{H_2}}{2}O_2+1.88(4-3\alpha_{H_2})N_2$$
$$=(1-\alpha_{H_2})CO_2+(2-\alpha_{H_2})H_2O+1.88(4-3\alpha_{H_2})N_2 \tag{R1}$$

and

$$(1-\alpha_{RG})CH_4+\alpha_{RG}\left(\frac{42}{205}CO+\frac{84}{205}H_2+\frac{79}{205}N_2\right)$$
$$+\left(2-2\alpha_{RG}+\frac{63\alpha_{RG}}{205}\right)O_2+3.76\left(2-2\alpha_{RG}+\frac{63\alpha_{RG}}{205}\right)N_2$$
$$=\left(1-\alpha_{RG}+\frac{42\alpha_{RG}}{205}\right)CO_2+\left(2-2\alpha_{RG}+\frac{84\alpha_{RG}}{205}\right)H_2O$$
$$+\left(7.52-\frac{1225.72\alpha_{RG}}{205}\right)N_2, \tag{R2}$$

respectively, for H_2 and RG addition. Note that N_2 in (R2) comes from two sources—RG and air.

3. Results and discussion

The fraction of hydrogen or RG in the fuel covers a range from 0.0 to 1.0 for completeness purpose.

3.1. Flame temperature variation

Fig. 2 shows the variation of the maximum flame temperature at strain rates (a) of 10, 100 and 300 s^{-1}, when hydrogen is added. The three values were selected to represent low, moderate and high strain rates. The highest one (300 s^{-1}) is close to the strain extinction limit for steady state pure methane/air diffusion flame at an atmospheric pressure and room temperature

condition. To explain the result, the adiabatic equilibrium flame temperatures (Adia. T), obtained by equilibrium calculation at stoichiometric condition (see (R1)) for each corresponding fuel composition, are also shown.

It is observed that the addition of hydrogen monotonically increases flame temperature at all strain rates. The first reason for this is the higher adiabatic equilibrium flame temperature of hydrogen relative to methane. However, it is noted that the rate of flame temperature increase is much faster than that of the adiabatic temperature at all strain rates, and the maximum temperatures at some α_{H_2} exceed the corresponding adiabatic equilibrium temperatures at a strain rate of 10 or 100 s^{-1}. This phenomenon is referred to as super-adiabatic temperature. The faster temperature increase and super-adiabatic temperature occur because of the second reason, the variation in fuel Lewis number, defined as the ratio of the thermal to mass diffusion rate. It is well known that for a diffusion flame, temperature is increased/decreased with decreasing/increasing Lewis number of either fuel or oxidant away from unity [23]. Ultra-low Lewis number sometimes causes a super-adiabatic temperature in a diffusion flame. The Lewis number of fuel in pure methane diffusion flames is close to unity, and hence has negligible effect on flame temperature. The Lewis number of hydrogen is significantly lower than unity. As a result, the fuel Lewis number is reduced to a value lower than unity, which tends to increase flame temperature and causes super-adiabatic temperature at some conditions as hydrogen is added. To confirm the Lewis number effect, we conducted extra calculations with the Lewis number artificially set to unity for all species at $a = 100$ s^{-1}. These results are also shown in Fig. 2. It is found that if there were not the Lewis number effect, the increase rate of flame temperature should have been similar to that of the adiabatic temperature, and the super-adiabatic temperature would not have occurred. Flames of other strain rates show similar results. Therefore, it is the effect of fuel Lewis number that results in the super-adiabatic temperature and the much faster increase of flame temperature than that of the adiabatic equilibrium temperature, when hydrogen is added.

It is also noted that at $a = 10$ s^{-1} and near $\alpha_{H_2} = 1.0$, the temperature increase rate slows down, and the maximum temperature becomes slightly lower than the adiabatic temperature again. This is because of radiation heat loss, which becomes more significant near $\alpha_{H_2} = 1.0$ due to the increased flame thickness. The impact of radiation heat loss decreases with increasing strain rate [24]. Therefore, the decreased temperature increase does not happen at $a = 100$ or 300 s^{-1}, and the maximum temperatures at $a = 100$ s^{-1} become higher than those at $a = 10$ s^{-1} when α_{H_2} is close to unity. Although not shown, the results of the calculation that neglected radiation heat loss do show that at $a = 10$ s^{-1}, the decreased temperature increase near $\alpha_{H_2} = 1.0$ does not happen and the maximum flame temperatures are always higher than those at $a = 100$ s^{-1}.

Being different from pure hydrogen, the adiabatic equilibrium temperature of pure RG is lower than that of pure methane at stoichiometric condition. Therefore, it was expected that the addition of RG would reduce the flame temperature. This has been shown to be true for near stoichiometric premixed flames [4]. However, the simulations here do not show such a result for diffusion flames, as shown in Fig. 3. At $a = 10$ s^{-1}, the addition of RG actually results in a monotonic increase in temperature. At $a = 300$ s^{-1}, the maximum temperature first increases, and then decreases, as α_{RG} increases. The situation at $a = 100$ s^{-1} is basically similar to that at $a = 300$ s^{-1}, except for a slight difference near $\alpha_{RG} = 1.0$, where the maximum temperature slightly rises again. Although the super-adiabatic temperature phenomenon does not happen for RG enriched flames, the maximum flame temperature is closer to the corresponding adiabatic value at $\alpha_{RG} = 1.0$ than at $\alpha_{RG} = 0$.

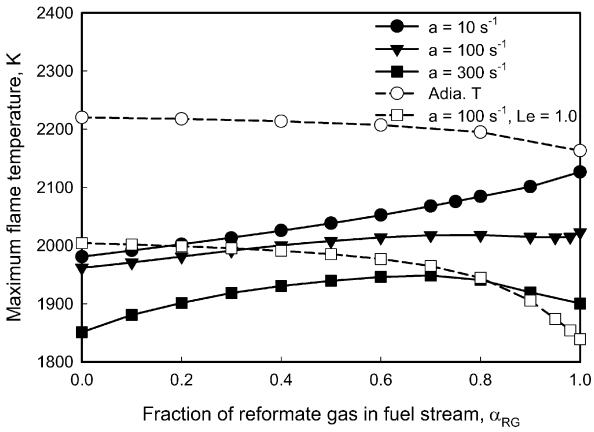

Fig. 3. Effect of RG addition on flame temperature. Solid lines with filled symbol: temperatures at different strain rates; Dashed line with open circle: equilibrium adiabatic temperature of the stoichiometric mixture (R2) at corresponding α_{RG}; Dashed line with open square: temperatures of flames at strain rate of 100 s^{-1} and with Le of all species being artificially set to unity.

These temperature variation phenomena with the addition of RG are also caused by the combination of the effects of adiabatic temperature and fuel Lewis number. Radiation heat loss effect is not significant for RG enriched flames, since the flame is not thick enough and temperature is not sufficiently high even at $a = 10$ s^{-1} and $\alpha_{RG} = 1.0$. Although the addition of RG tends to reduce flame temperature owing to the variation in adiabatic flame temperature, it also changes the fuel Lewis number. The fuel stream consists of methane, hydrogen, carbon monoxide and nitrogen in RG enriched flames. The Lewis numbers of methane, carbon monoxide and nitrogen are close to unity, but that of hydrogen is significantly lower. Consequently, the fuel Lewis number is reduced to a value lower than unity. The temperature variation of a flame depends on the balance between the effects of adiabatic temperature and Lewis number. This is also confirmed by the calculations with the Lewis number artificially set to unity for all species at $a = 100$ s^{-1}. We see that flame temperature would have monotonically decreased if Le = 1.0.

At $a = 10$ s^{-1}, the effect of Lewis number is stronger than that of the reduction in adiabatic flame temperature, leading to a monotonic temperature increase. The effect of Lewis number becomes weaker with increasing strain rate. At $a = 100$ or 300 s^{-1}, when α_{RG} is not big enough, the effect of Lewis number is still stronger than that of the adiabatic flame temperature, resulting in a temperature increase. However, further increasing α_{RG} reverses the relative effects of the Lewis number and adiabatic temperature, which leads to a reduction in flame temperature. The slight temperature increase at $a = 100$ s^{-1} and near $\alpha_{RG} = 1.0$ is due to the Lewis number effect becoming stronger again when a large amount of hydrogen exists in the fuel mixture. However, this slight temperature increase phenomenon does not happen at $a = 300$ s^{-1}, since the Lewis number effect is further weakened.

The super-adiabatic temperature does not happen in RG enriched flames, because the hydrogen content is not big enough. As noted from the composition of the RG, the volume fraction of H_2 in the pure RG is about 0.41. Fig. 2 indicates that super-adiabatic temperature appears when α_{H_2} is greater than 0.7 at strain rate of 10 or 100 s^{-1}.

Therefore, the effect of Lewis number significantly affects flame temperature when hydrogen or RG is added to a methane/air diffusion flame. In the application of fuel enrichment combustion technology, this effect should be carefully taken into account.

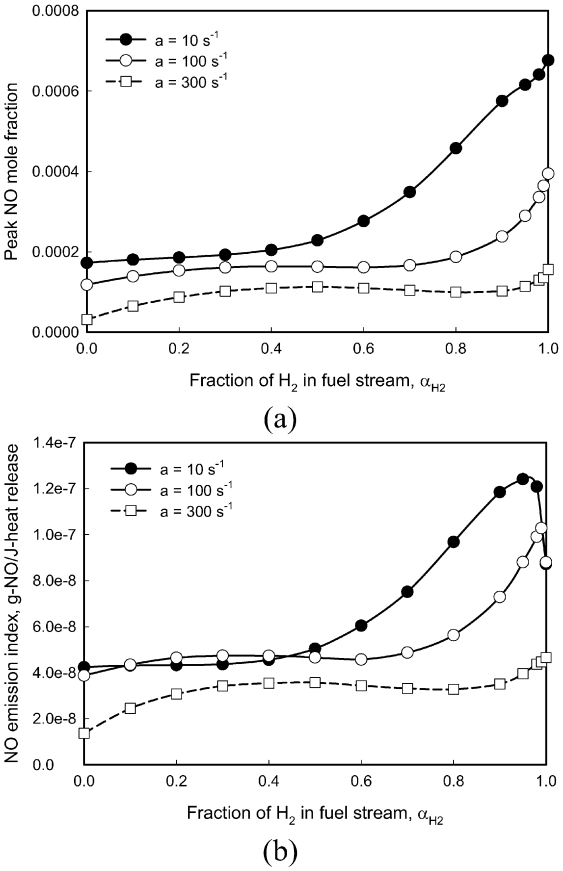

Fig. 4. Effect of hydrogen addition on NO formation. (a) Peak NO mole fraction; (b) NO emission index.

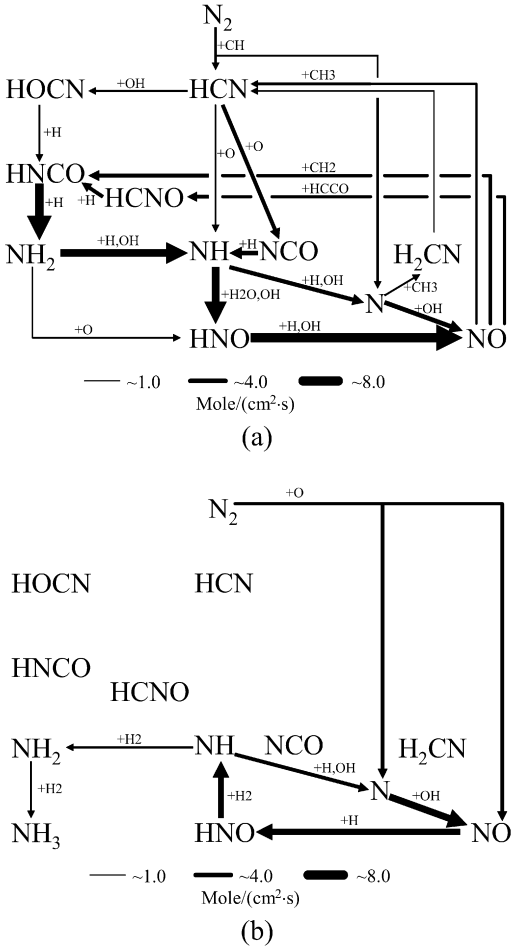

Fig. 5. NO formation pathway at $a = 10\ s^{-1}$. (a) CH_4/air flame; (b) H_2/air flame.

3.2. NO formation in hydrogen enriched flames

Fig. 4 displays the variations of peak NO mole fraction and NO emission index, defined as the ratio of NO formed to total heat release (g-NO/J-heat). It is revealed that at a given strain rate, although the maximum temperature monotonically increases, the behaviors of NO emission index and peak NO mole fraction are complex, as α_{H_2} increases. Moreover, the variation trends differ at different strain rates.

At $a = 10$ or 100 s^{-1}, there is a critical α_{H_2} between 0.0 and 1.0, at which NO emission index reaches its maximum value. The value of the critical α_{H_2} is higher at $a = 100\ s^{-1}$ than at $a = 10\ s^{-1}$. However, such a critical α_{H_2} does not exist or becomes 1.0 at $a = 300\ s^{-1}$. The peak NO mole fraction always reaches its maximum value at $\alpha_{H_2} = 1.0$, regardless of the variation in strain rate.

At $a = 10\ s^{-1}$, both NO emission index and the peak NO mole fraction are fairly constant as α_{H_2} increases from 0.0 to 0.4, and then quickly increase until the maximum NO emission index is reached at the critical α_{H_2} (about 0.95). Finally, further increasing α_{H_2} from the critical value to 1.0, the NO emission index decreases, while the peak NO mole fraction increases.

The situation changes at $a = 100$ or 300 s^{-1}. When a small amount of hydrogen is added, both peak NO mole fraction and NO emission index increase. The increase is more significant at $a = 300\ s^{-1}$ than at $a = 100\ s^{-1}$. Then the increase of α_{H_2} causes a slight decrease in both peak NO mole fraction and NO emission index. Finally, further increasing α_{H_2}, both parameters quickly rise until the critical α_{H_2} (0.98) is reached at $a = 100\ s^{-1}$, or $\alpha_{H_2} = 1.0$ is reached at $a = 300\ s^{-1}$. When α_{H_2} is greater than the critical value, the variations of the two parameters at $a = 100\ s^{-1}$ are qualitatively similar to those at $a = 10\ s^{-1}$. At $a = 300\ s^{-1}$, they both reach their maximum at $\alpha_{H_2} = 1.0$.

The above phenomena can be explained by the variations in the mechanisms of NO formation and flame structure. It is known that NO generally can be formed by the thermal, the prompt, the N_2O and NNH intermediate routes in a hydrocarbon flame [25,26]. Fig. 5 displays the pathways of NO formation in pure methane/air and hydrogen/air diffusion flames with $a = 10\ s^{-1}$. The paths with rates less than 1.0×10^{-8} mol/(cm^3 s) have been neglected. The species not participating in any reaction in the hydrogen/air flame are still kept for comparison. It is observed that most NO is formed by the paths HNO (+H, OH) → NO and N (+OH) → NO in the methane/air flame, and by N (+OH) → NO and N_2 (+O) → NO in the hydrogen/air flame. Apparently, the path HNO (+H, OH) → NO in the methane/air flame belongs to the prompt route, since species HNO is from the paths resulting from the reaction of molecular nitrogen with CH radical. Although both flames share the path N (+OH) → NO, the atomic nitrogen in this path of the two flames comes from different sources. In the methane/air flame, it is from the paths resulting from the reaction $N_2 + CH = HCN + N$ that is the typical prompt route nitrogen conversion reaction [26]. On the other hand, in the hydrogen/air diffusion flame, the atomic nitrogen is from the reverse reaction of $N + NO = N_2 + O$ that is the thermal route. This observation suggests that the method to identify the mechanism of NO formation in a flame should not be based on how NO is finally formed, but on how molecular nitrogen is initially converted to atomic nitrogen or nitrogen-containing species. For the sake of simplification, we examine the mechanism of NO formation of other flames according

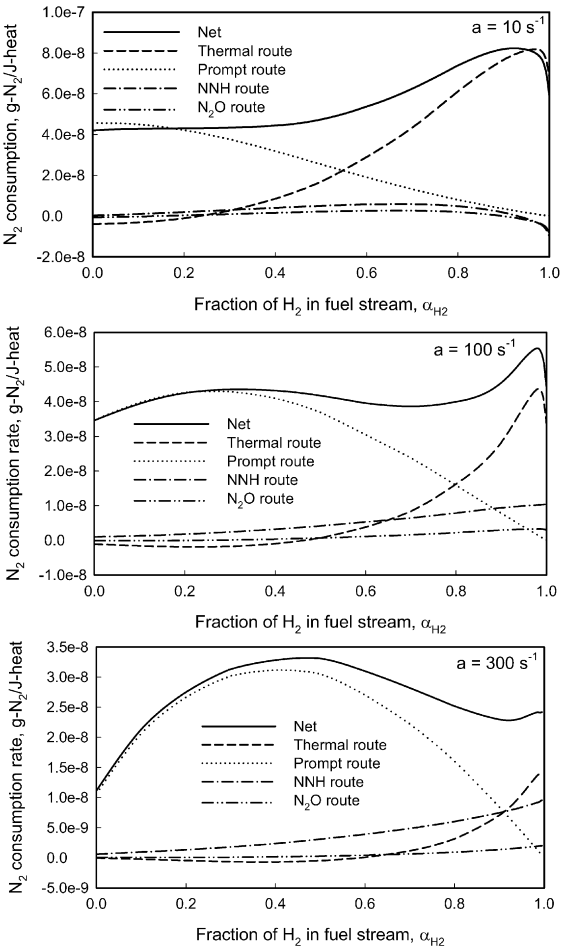

Fig. 6. Nitrogen consumption rates of hydrogen enriched flames.

to the consumption rates of molecular nitrogen, rather than the final formation of NO.

Fig. 6 displays the molecular nitrogen consumption rates by different routes in flames at the three typical strain rates. Similar to NO emission index, the nitrogen consumption rate is defined as the ratio of total consumed N_2 to total heat release (g-N_2/J-heat). A positive value means nitrogen is converted to NO or nitrogen-containing species, and a negative value indicates the opposite. For completeness, the nitrogen consumption rates by the N_2O and NNH intermediate routes are also shown. However, their variations will not be discussed since the contributions are generally very small. The identification method of the nitrogen consumption by different routes may be found elsewhere [3,4]. It is observed that at $\alpha_{H_2} = 0.0$, the prompt route dominates the conversion of nitrogen at all strain rates. The consumption rate of nitrogen by the thermal route is slightly negative at $\alpha_{H_2} = 0.0$ because a large amount of atomic nitrogen is formed by the reaction $N_2 + CH = HCN + N$, resulting in the forward rate of the reaction $NO + N = N_2 + O$ exceeding the reverse rate. Alternatively, the thermal route contributes most at $\alpha_{H_2} = 1.0$. The combination of the variations in the nitrogen consumption rates by the thermal and prompt routes explains most of the phenomena observed in Fig. 4.

At $a = 10\ s^{-1}$, the consumption rates of nitrogen by the thermal and prompt routes increase and decrease, respectively, leading to a nearly constant net nitrogen consumption rate and NO emission index, as α_{H_2} increases from 0.0 to 0.4. Further increasing α_{H_2} from 0.4 to the critical value, the consumption rate of nitrogen by the thermal route quickly increases, while that by the prompt route gradually decreases, resulting in an increase in net nitrogen consumption rate and NO emission index. The monotonic decrease of nitrogen consumption rate by the prompt route is due to the decrease in the concentration of CH radical, as shown in Fig. 7. For the thermal route, when α_{H_2} increases from 0.0 to the critical value, the increase of nitrogen consumption rate is caused by the increase in temperature. When α_{H_2} approaches unity, the final decrease in nitrogen consumption rate and NO emission index is caused by the decrease in the consumption of nitrogen by the thermal route. This will be further explained later.

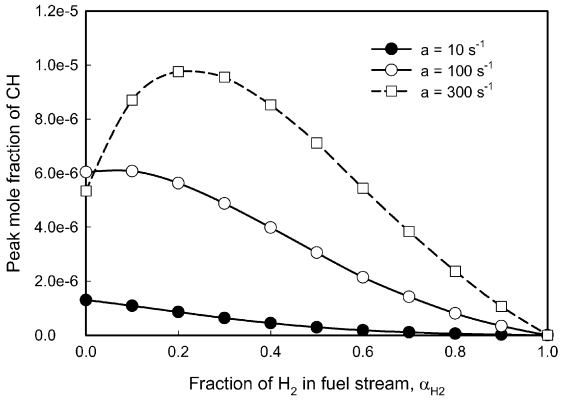

Fig. 7. Variation of peak CH mole fraction.

At $a = 300\ s^{-1}$, as α_{H_2} first increases from 0.0 to a certain value, the consumption rate of nitrogen by the prompt route increases, while that by the thermal route is almost constant, leading to increases in net nitrogen consumption rate and NO emission index. At this stage, the almost constant nitrogen consumption rate by the thermal route is due to the net effects of the temperature increase that tends to raise the nitrogen consumption rate by the thermal route, and the rise in the nitrogen consumption by the prompt route that generates a large amount of atomic nitrogen and thus intensifies the forward rate of the reaction $NO + N = N_2 + O$. The increase in the consumption rate of nitrogen by the prompt route is caused by the fact that a small amount of hydrogen addition increases the concentration of CH radical, as shown in Fig. 7, because the addition of hydrogen intensifies the fuel decomposition rate of a methane/air diffusion flame if the strain rate is not very low. This effect does not happen at a lower strain rate, such as at $a = 10\ s^{-1}$, since the residence time of reactants in the reaction zone of a lower strain rate flame is long enough to complete the combustion process, and thus the addition of hydrogen only increases temperature and reduces the concentration of CH radical. With α_{H_2} being increased beyond a certain value, the concentration of CH radical starts to decrease, resulting in a reduction in the consumption rate of nitrogen by the prompt route and NO emission index. Finally, further increasing α_{H_2} to 1.0, the nitrogen consumption rate by the thermal route and thus the net nitrogen consumption and NO emission index increase again due to the significantly increased temperature.

The result at $a = 100\ s^{-1}$ is qualitatively similar to that at $a = 300\ s^{-1}$, except that there is a critical α_{H_2} (0.98). When α_{H_2} is greater than the critical value, the result at $a = 100\ s^{-1}$ is qualitatively similar to that at $a = 10\ s^{-1}$, i.e. the increase of α_{H_2} reduces the nitrogen consumption rate and NO emission index, while increasing the peak NO mole fraction, as shown in Fig. 4. This is because the reaction zone is moved further away from the stagnation plane at a higher α_{H_2}. The formation of NO in the primary reaction zone keeps increasing because of the rise in temperature, resulting in an increase in peak NO mole fraction. However, when the formed NO is transported to the region close to stagnation plane, part of the NO is converted back to molecular nitrogen by the reaction $NO + N = N_2 + O$, leading to a decrease in NO emission

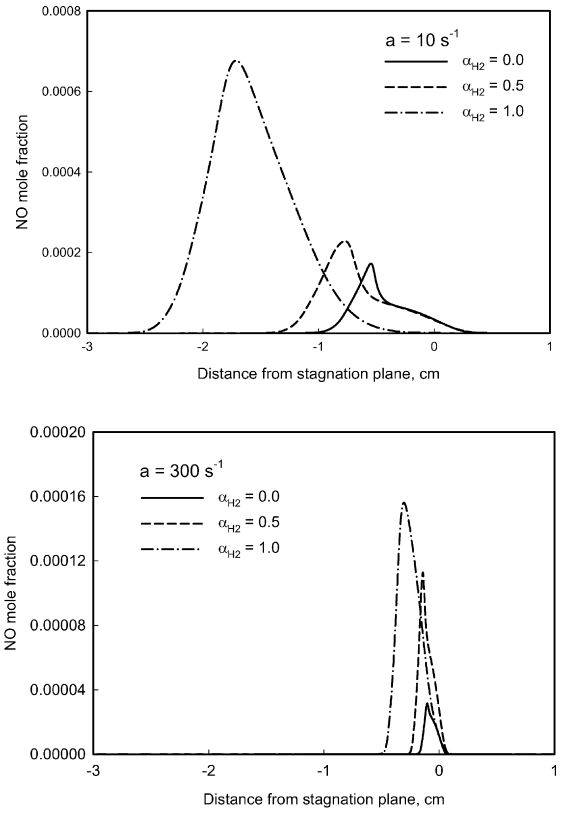

Fig. 8. NO mole fraction distribution at strain rates of 10 and 300 s^{-1}.

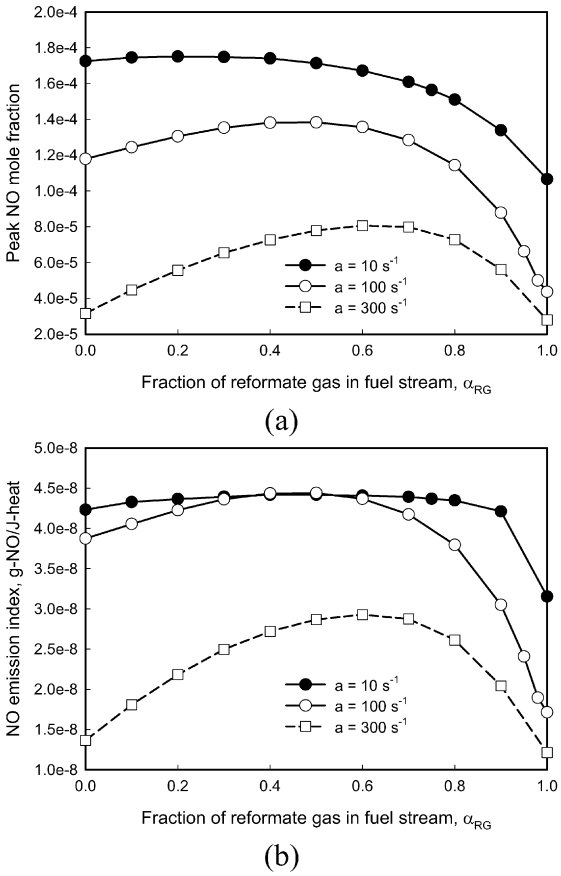

Fig. 9. Effect of RG addition on NO formation. (a) Peak NO mole fraction; (b) NO emission index.

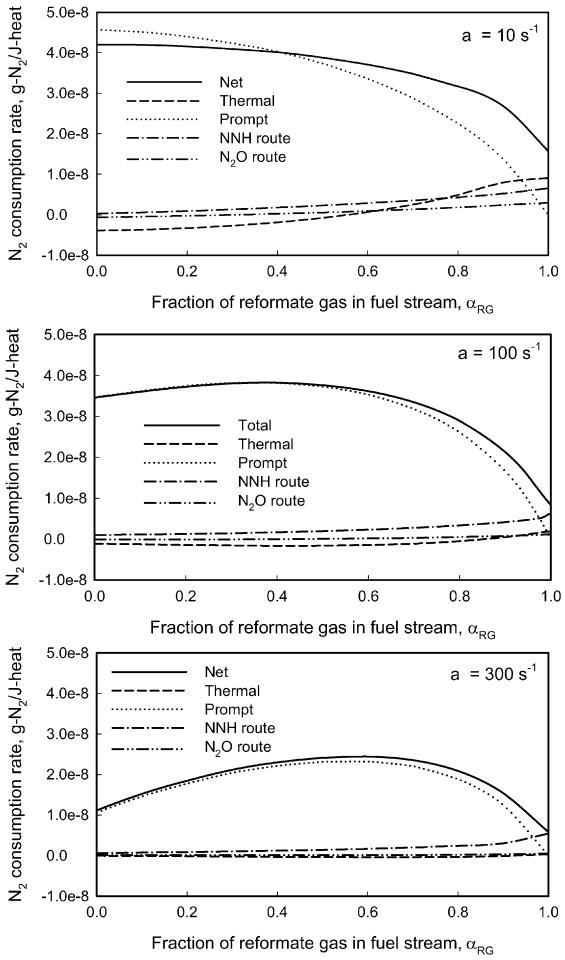

Fig. 10. Nitrogen consumption rates of RG enriched flames.

index. This phenomenon does not happen at $a = 300$ s^{-1}, since the reaction zone is closer to the stagnation plane at all α_{H_2}. The location of primary reaction zone at different α_{H_2} and strain rates can be observed from the distribution of NO mole fraction in Fig. 8.

3.3. NO formation in RG enriched flames

Fig. 9 shows the variations of peak NO mole fraction and NO emission index when RG is added. At $a = 10$ s^{-1}, although temperature monotonically increases (Fig. 3), both peak NO mole fraction and NO emission index first are almost constant and then decrease, when α_{RG} is increased. At $a = 100$ or 300 s^{-1}, both parameters vary in a slightly different way from $a = 10$ s^{-1}. They first increase and then decrease, but the critical α_{RG} at which the maximum is reached varies with strain rate.

Fig. 10 shows the variation of molecular nitrogen consumption rates at the three typical strain rates. At $a = 10$ s^{-1}, the nitrogen consumption rates by the thermal and prompt routes increase and decrease, respectively, leading to a relatively constant net nitrogen consumption rate and NO emission index, as α_{RG} increases from 0.0 to a moderate value. The increase and decrease in the nitrogen consumption rates by the thermal and prompt routes are because of the increase in temperature and reduction in the concentration of CH radical, respectively. Further increasing α_{RG}, the nitrogen consumption rate by the prompt route quickly decreases. On the other hand, although the consumption rate of nitrogen by the thermal route increases due to temperature rise, the increase rate is much smaller than the decrease rate of the prompt route. Consequently, the net nitrogen consumption rate decreases as α_{RG}

increases from a moderate value to unity, resulting in a reduction in peak NO mole fraction and NO emission index.

At $a = 300\ s^{-1}$, as α_{RG} first increases from 0.0 to a certain value, the nitrogen consumption rate by the prompt route increases, while that by the thermal route is almost constant, leading to an increase in net nitrogen consumption rate. This results in the increase in peak NO mole fraction and NO emission index. Similar to hydrogen addition, the almost constant nitrogen consumption rate by the thermal route is due to the net effects of the temperature increase and the rise in the nitrogen consumption rate by the prompt route that intensifies the forward rate of the reaction $NO + N = N_2 + O$. The increase in the nitrogen consumption rate by the prompt route is because the addition of a small amount of RG intensifies the combustion due to hydrogen and CO, and thus the concentration of CH radical is actually increased. The increase in both CH concentration and temperature causes the increase in nitrogen consumption rate by the prompt route. Further increasing α_{RG} beyond a certain value, the concentration of CH radical and flame temperature start to decrease, resulting in the reduction in nitrogen consumption rate by the prompt route and hence peak NO mole fraction and NO emission index. The change in the nitrogen consumption rate by the thermal route is still negligible at this later stage, although the temperature reduces with increasing α_{RG}. This is because the effect of atomic nitrogen produced by the prompt route on the forward reaction $NO + N = N_2 + O$ decreases.

The result at $a = 100\ s^{-1}$ is qualitatively similar to that at $a = 300\ s^{-1}$. The slight temperature increase near $\alpha_{RG} = 1.0$ at $a = 100\ s^{-1}$ is not enough to cause an increase in net NO formation rate.

4. Conclusions

A detailed numerical study on the effect of hydrogen/RG enrichment on flame temperature and NO formation in strained CH_4/air diffusion flames has been conducted. The results indicate that when hydrogen or RG is added, the variations in both the adiabatic flame temperature and the fuel Lewis number significantly affect the flame temperature. Because of the Lewis number effect, the flame temperature increases much faster than the adiabatic equilibrium temperature, and a super-adiabatic flame temperature occurs at some conditions, when α_{H_2} is increased. As for the addition of RG, the Lewis number effect can result in a qualitatively different flame temperature trend from that of the adiabatic temperature. Therefore, the Lewis number effect has to be carefully taken into account in the application of hydrogen or RG enrichment technology.

The addition of a small amount of hydrogen or RG has negligible effect on NO formation in a methane/air diffusion flame at low strain rates. At moderate or high strain rates, the addition of a small amount hydrogen or RG leads to a small increase in NO formation. Considering the fact that the absolute NO formation rate at moderate to high strain rates is usually low, we can say that the addition of a small amount of hydrogen or RG has a minor effect on NO formation. However, the addition of a large amount of hydrogen or RG results in an increase or decrease in NO formation, except that a complex phenomenon occurs near pure hydrogen condition.

Acknowledgment

The financial support of the Government of Canada's PERD/AFTER program is gratefully acknowledged.

References

[1] G.S. Jackson, R. Sai, J.M. Plaia, C.M. Boggs, K.T. Kiger, Combust. Flame 132 (2003) 503–511.
[2] J.Y. Ren, W. Qin, F.N. Egolfopoulos, H. Mak, T.T. Tsotsis, Chem. Eng. Sci. 56 (2001) 1541–1549.
[3] H. Guo, G.J. Smallwood, F. Liu, Y. Ju, Ö.L. Gülder, Proc. Combust. Inst. 30 (2005) 303–311.
[4] H. Guo, G.J. Smallwood, Ö.L. Gülder, Proc. Combust. Inst. 31 (2007) 1197–1204.
[5] R. Sankaran, H.G. Im, Combust. Sci. Technol. 178 (2006) 1585–1611.
[6] G. Yu, C.K. Law, C.K. Wu, Combust. Flame 63 (1986) 339–347.
[7] Z. Huang, Y. Zhang, K. Zeng, B. Liu, Q. Wang, D. Jiang, Combust. Flame 146 (2006) 302–311.
[8] F.H.V. Coppens, J.D. Ruyck, A.A. Konnov, Combust. Flame 149 (2007) 409–417.
[9] Ö.L. Gülder, D.R. Snelling, R.A. Sawchuk, Proc. Combust. Inst. 26 (1996) 2351–2358.
[10] H. Guo, F. Liu, G.J. Smallwood, Ö.L. Gülder, Combust. Flame 145 (2006) 324–338.
[11] Y. Ju, T. Niioka, Combust. Flame 99 (1994) 240–246.
[12] G.G. Fotache, T.G. Kreutz, C.K. Law, Combust. Flame 110 (1997) 429–440.
[13] S. Naha, S.K. Aggarwal, Combust. Flame 139 (2004) 90–105.
[14] V.S. Santoro, D.C. Kyritsis, M.D. Smooke, A. Gomez, Proc. Combust. Inst. 29 (2002) 2227–2233.
[15] V. Giovangigli, M.D. Smooke, Combust. Sci. Technol. 53 (1987) 23–49.
[16] R.J. Kee, J.F. Grcar, M.D. Smooke, J.A. Miller, A Fortran Program for Modeling Steady Laminar One-Dimensional Premixed Flames, Report No. SAND 85-8240, Sandia National Laboratories, 1985.
[17] H. Guo, Y. Ju, K. Maruta, T. Niioka, F. Liu, Combust. Flame 109 (1997) 639–646.
[18] G.P. Smith, D.M. Golden, M. Frenklach, N.W. Moriarty, B. Eiteneer, M. Goldenberg, C.T. Bowman, R.K. Hanson, S. Song, W.C. Gardiner Jr., V.V. Lissianski, Z. Qin, available at http://www.me.berkeley.edu/gri_mech/.
[19] S.V. Naik, N.M. Laurendeau, Combust. Sci. Technol. 176 (2004) 1809–1853.
[20] A.V. Menon, S.-Y. Lee, M.J. Linevsky, T.A. Litzinger, R.J. Santoro, Proc. Combust. Inst. 31 (2006) 593–601.
[21] R.J. Kee, J. Warnatz, J.A. Miller, A Fortran Computer Code Package for the Evaluation of Gas-Phase Viscosities, Conductivities, and Diffusion Coefficients, Report No. SAND 83-8209, Sandia National Laboratories, 1983.
[22] R.J. Kee, J.A. Miller, T.H. Jefferson, A General-Purpose, Problem-Independent, Transportable, Fortran Chemical Kinetics Code Package, Report No. SAND 80-8003, Sandia National Laboratories, 1980.
[23] C.K. Law, S.H. Chung, Combust. Sci. Technol. 29 (1982) 129–145.
[24] K. Maruta, Y. Yoshida, H. Guo, Y. Ju, T. Niioka, Combust. Flame 112 (1998) 181–187.
[25] J.W. Bozzelli, A.M. Dean, Int. J. Chem. Kinet. 27 (1995) 1097–1109.
[26] J.A. Miller, C.T. Bowman, Prog. Energy Combust. Sci. 15 (1989) 287–338.